



A numerical study of mixed convection heat transfer in a lid-driven cavity using Al_2O_3 -water nanofluid

Neşe KEKLİKÇİOĞLU ÇAKMAK^{1,*}, Hasan H. DURMAZUÇAR¹, Kerim YAPICI²

on the last page

¹Department of Chemical Engineering, Faculty of Engineering, Sivas Cumhuriyet University, Sivas, Turkey,

²Department of Chemical Engineering, Faculty of Engineering, Süleyman Demirel University, Isparta, Turkey

Received: 03 March 2020; Revised: 15 March 2020; Accepted: 16 March 2020

*Corresponding author e-mail: nkeklkcioglu@cumhuriyet.edu.tr

Citation: Keklikcioglu Cakmak, N.; Durmazucar, H. H.; Yapici, K. *Int. J. Chem. Technol.* 2020, 4 (1), 22-37.

ABSTRACT

This study aims a numerical investigation of steady, laminar mixed convection heat transfer in a two-dimensional cavity by employing a finite volume method with a fourth-order approximation of convective terms, when nanoparticles are present. With the aim of solving two-dimensional momentum and energy conservation equations, a finite volume method on a non-uniform staggered grid is utilized. Second-order central differences are utilized to approximate diffusion terms in momentum and energy equations, while the development of a non-uniform four-point fourth-order interpolation (FPFOI) scheme is performed for the convective terms. Continuity and momentum equations are solved using the SIMPLE (Semi-Implicit Method for Pressure-Linked Equation) algorithm. In order to evaluate heat transfer enhancement, various viscosity and thermal conductivity models were employed. Numerical solution results were obtained in different models in cases where Gr number is between 10^3 and 10^5 , Re number is 10-100-1000 and nanoparticle volumetric fraction is 0-5%.

Keywords: Nanofluid, finite volume method, fourth-order linear scheme, lid-driven cavity, mixed convection.

Al_2O_3 -su nanoakışkan kullanılarak kapak tahrikli düzgün dörtgen boşluk içerisinde karışık konveksiyon ısı aktarımın sayısal olarak incelenmesi

Öz

Bu çalışma nanoparçacıklar varlığında konvektif terimlerin dördüncü dereceden doğruluğa sahip sonlu hacimler yöntemi kullanılarak iki boyutlu sistemlerde yatışkın, laminar karışık konveksiyon ısı aktarımının sayısal olarak incelenmesini amaçlamaktadır. İki-boyutlu momentum ve enerji tasarrufu eşitliklerini çözüme amacı ile düzgün dağılımlı olmayan yapısal kaydırılmış ızgara yapısında sonlu hacimler yöntemi kullanılmıştır. Konvektif terimler için düzgün dağılımlı olmayan ağ yapılarında dördüncü dereceden doğruluğa sahip (FPFOI) şemanın geliştirilmesi gerçekleştirilirken ikinci dereceden merkezi farklar, momentum ve enerji eşitlikleri içerisindeki yaklaşık difüzyon terimleri için kullanılmıştır. Süreklilik ve momentum denklemleri basit (Basınca Bağlı denklem için yarı örtük yöntem) algoritma kullanılarak çözülmüştür. Isı aktarım artışı değerlendirmek için çeşitli viskozite ve ısı iletkenlik modelleri kullanılmıştır. Gr sayısı 10^3 ve 10^5 aralığında, Re sayısı 10-100-1000 ve nanoparçacık hacimsel fraksiyonu % 0-5 olduğu durumlarda farklı modellerde sayısal çözüm sonuçları elde edilmiştir.

Anahtar Kelimeler: Nanoakışkan, sonlu hacimler yöntemi, dördüncü dereceden doğrusal şema, kapak tahrikli düzgün dörtgen boşluk, karışık konveksiyon.

1. INTRODUCTION

Because of the quick advancements experienced in computer technology and computational sciences,

computational fluid dynamics (CFD) has turned into a significant instrument in industrial and scientific research activities. It is possible to indicate the comparatively significant costs and considerable

DOI: <http://dx.doi.org/10.32571/ijct.697728>

E-ISSN:2602-277X

time requirements of experimental research and occasionally unpractical conditions of experiments among the primary causes promoting numerical CFD research. Natural and mixed convection heat transfer is involved in various engineering applications, including the cooling of electronic devices, solar collectors, building insulation, etc. Since there are numerous applications of natural and mixed convection heat transfer in engineering, there is a lot of numerical and experimental research on the mentioned transport processes in the scientific literature.¹ Tiwari and Das² published the first research on the mixed convection of nanofluids in enclosures. The researchers conducted the numerical investigation of the heat transfer improvement in a two-sided lid-driven square cavity utilizing nanofluids. They employed a finite volume approach by utilizing the SIMPLE (Semi-Implicit Method for Pressure-Linked Equation) algorithm. They presented a summary of a number of significant observations in the following way. The average Nusselt number changes nonlinearly with the solid volume fraction, nanoparticles can alter the fluid's flow pattern from natural convection to the forced convection regime, and the highest Nusselt number improvement is approximately 100%. Talebi and co-workers³ investigated the mixed convection of nanofluids in a laminar flow with the volume fraction of $\varphi = 0 - 0.05$ in an enclosure. The Patel and Brinkman models have been employed for the estimation of the thermal conductivity and effective dynamic viscosity of nanofluids, respectively. It has been understood that enhancement will occur in the flow function with the increased Reynolds number at every nanoparticle concentration, particularly at higher Rayleigh numbers. Furthermore, it has been determined that a decrease occurs in the impact of nanoparticle concentration with the increased Reynolds number, particularly at lower Rayleigh numbers.

Arefmanesh and Mahmoodi⁴ examined the impact of non-effective dynamic viscosity with nanoparticle volume fractions of $\varphi = 0; 0:1; 0:06; 0:03$ in laminar flow mixed convection and heat transfer in a square enclosure. The finite volume method and SIMPLE algorithm have been employed for the numerical solution of the governing equations, and two various models suggested by Brinkman⁵ and Maiga and co-workers⁶ have been utilized for nanofluid effective dynamic viscosity. Forced convection in an enclosure has been acquired as a result of moving the enclosure's lower wall, whereas natural convection has been occurred in case of a higher temperature of the enclosure's lower wall in comparison with its other walls. There is a strong dependence of the uncertainty impacts in the viscosity formula for water- Al_2O_3 nanofluid on the Richardson number and nanoparticle volume fraction. Chamkha and co-workers⁷ have

carried out the numerical investigation of the impacts of partial slip on the generation of entropy magnetohydrodynamics (MHD) combined convection in a square lid-driven porous enclosure that was saturated with Cu-water nanofluids. The result they have obtained demonstrates that an augmentation in the heat generation/absorption parameter causes a decrease in the Nusselt number. Moreover, with the increased volume fraction, a decrease in the Nusselt number and entropy generation takes place. In a recent numerical study carried out by Kapil and co-workers⁸ has been investigated mixed convection heat transfer of the Al_2O_3 - water nanofluid in a lid driven cavity with heated square obstacle at the center. They have used the upwind scheme to solve the set of equations. Three different Re (1, 10 and 100) numbers in the fixed Gr (10^4) number has also been studied, and in addition to these, it has been not specified what correlation equation of Al_2O_3 -water nanofluid viscosity has been modeled. They have concluded that while Nusselt number increases with increasing Re numbers, it decreases at low Re numbers. The current study primarily aims to examine the mixed convection heat transfer in a lid-driven cavity using nanofluids. Al_2O_3 -water nanofluids and three variable viscosity and thermal conductivity models have been utilized for the purpose of investigating the impact of nanoparticles on the mixed convection flow and temperature fields, and comprehensive research has been conducted on the used model of the nanofluid together with other parameters that determines the flow pattern. In our study, to approximate the diffusion terms in the governing equations, the second-order central differencing scheme is used. The non-uniform form of the four-point fourth-order interpolation (FPFOI) scheme is used to approximate the convective terms. In this respect, our study is different from the studies mentioned above, and no similar studies has been found in the literature in terms of different Re and Gr number, viscosity and thermal conductivity models and equations used.

2. PROBLEM STATEMENT AND MATHEMATICAL FORMULATION

Figure 1 presents the mentioned physical models, along with the corresponding boundary conditions and geometric dimensions. This figure clearly demonstrates the boundary conditions used for velocity and temperature and the flow geometry, in which the upper wall moves at a certain constant velocity, the other walls are motionless, the lower wall is heated, the upper wall is cooled, and the other walls are insulated. In this study, the results with fourth-order accuracy are given at different Grashof (Gr) and Reynolds (Re) numbers. The thermophysical parameters of Al_2O_3 nanoparticles and water are given in Table 1.^{9,10}

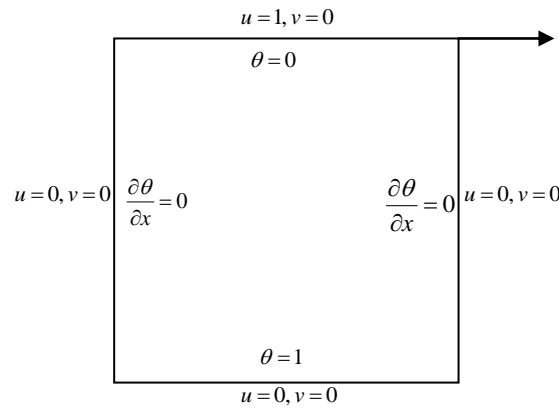


Figure 1. Both natural and forced convection heat transfer flow geometry and dimensionless velocity and temperature boundary conditions.

Table 1. Thermophysical parameters of Al₂O₃ nanoparticles and water

	ρ (kg m ⁻³)	C_p (Jkg ⁻¹ K ⁻¹)	k (W m ⁻¹ K ⁻¹)	μ (kgm ⁻¹ s ⁻¹)	β (K ⁻¹)
Al ₂ O ₃	3970	765	40	-	0.85×10 ⁻⁵
Water	997-1	4170	0.613	0.001	21×10 ⁻⁵

Furthermore, the solution of natural and mixed convection problems is performed with Al₂O₃-water nanofluid as a working fluid. In order to solve the Al₂O₃-water nanofluid, the homogeneous single-phase

approach is accepted, and thus, the Al₂O₃-water nanofluid takes the place of the physical characteristics of the Newtonian fluid mentioned above.

$$\frac{\partial u}{\partial x} + \frac{\partial v}{\partial y} = 0 \tag{1}$$

$$u \frac{\partial u}{\partial x} + v \frac{\partial v}{\partial y} = -\frac{1}{\rho_{nf}} \frac{\partial p}{\partial x} + \nu_{nf} \left(\frac{\partial^2 u}{\partial x^2} + \frac{\partial^2 u}{\partial y^2} \right) \tag{2}$$

$$u \frac{\partial v}{\partial x} + v \frac{\partial v}{\partial y} = -\frac{1}{\rho_{nf}} \frac{\partial p}{\partial y} + \nu_{nf} \left(\frac{\partial^2 v}{\partial x^2} + \frac{\partial^2 v}{\partial y^2} \right) + g\beta_{nf} (T - T_c) \tag{3}$$

$$u \frac{\partial T}{\partial x} + v \frac{\partial T}{\partial y} = \alpha_{nf} \left(\frac{\partial^2 T}{\partial x^2} + \frac{\partial^2 T}{\partial y^2} \right) \tag{4}$$

It is possible to write the non-dimensional governing equations in the following way, where the subscript *nf* denotes the characteristics of the Al₂O₃-water nanofluid,

and the subscript *f* refers to the features of the base fluid (water):

$$x' = \frac{x}{H}, \quad y' = \frac{y}{H}, \quad u' = \frac{uH}{\alpha_f}, \quad v' = \frac{vH}{\alpha_f}, \quad p' = \frac{pH^2}{\rho_{nf}\alpha_f^2}, \quad \theta = \frac{T - T_C}{T_H - T_C} \quad (5)$$

$$\frac{\partial u'}{\partial x'} + \frac{\partial v'}{\partial y'} = 0 \quad (6)$$

$$u' \frac{\partial u'}{\partial x'} + v' \frac{\partial v'}{\partial y'} = -\frac{\partial p'}{\partial x'} + \frac{1}{Re} \left(\frac{\partial^2 u'}{\partial x'^2} + \frac{\partial^2 u'}{\partial y'^2} \right) \quad (7)$$

$$u' \frac{\partial v'}{\partial x'} + v' \frac{\partial v'}{\partial y'} = -\frac{\partial p'}{\partial y'} + \frac{1}{Re} \left(\frac{\partial^2 v'}{\partial x'^2} + \frac{\partial^2 v'}{\partial y'^2} \right) + Ri\theta \quad (8)$$

$$u' \frac{\partial \theta}{\partial x'} + v' \frac{\partial \theta}{\partial y'} = \frac{1}{Re Pr} \left(\frac{\partial^2 \theta}{\partial x'^2} + \frac{\partial^2 \theta}{\partial y'^2} \right) \quad (9)$$

The governing equations presented above are acquired by utilizing the following non-dimensional quantities: The dimensionless Reynolds (*Re*), Prandtl (*Pr*),

Richardson (*Ri*) and Grashof (*Gr*) numbers are presented in Eq. (10).

$$Re = \frac{\rho u_{lid} H}{\mu} \quad Pr = \frac{C_p \mu}{k} \quad Ri = \frac{Gr}{Re^2} \quad Gr = \frac{g\beta(T_H - T_C)H^3}{\nu^2} \quad (10)$$

The finite volume method is employed for the discretization of the governing flow equations. approximate the diffusion terms in the governing equations, the second-order central differencing scheme is used. At the same time, the non-uniform form of FPFOI scheme suggested by Yapici and Obut¹¹ is used

to approximate the convective terms. In the literature, there are different relations introduced for the physical characteristics of the Al₂O₃-water nanofluid. In the current paper, an investigation of three various viscosity and thermal conductivity correlation model equations given in Table 2 was carried out.

Table 2. Thermal conductivity and viscosity models utilized in numerical analysis

Model	Researcher	Viscosity	Thermal conductivity
I	(Einstein) ¹²	$\frac{\mu_{nf}}{\mu_f} = (1 + 2.5\phi)$ b = 5300, n = 2.8	$\frac{k_{nf}}{k_f} = \frac{(k_p + 2k_f) - 2\phi(k_f - k_p)}{(k_p + 2k_f) - \phi(k_f - k_p)}$ (Maxwell) ¹³
II	(Chandrasekar and co-workers) ¹⁴	$\frac{\mu_{nf}}{\mu_f} = \left(1 + b \left(\frac{\phi}{1 - \phi} \right)^n \right)$	
III	This study (Experimentally)	$\frac{\mu_{nf}}{\mu_f} = (1 + 2.5\phi + 107.2\phi^2)$	

DOI: <http://dx.doi.org/10.32571/ijct.697728>

E-ISSN:2602-277X

where ϕ refers to the volume fraction of Al_2O_3 nanoparticles in water, the base fluid. The mixing rule is used to evaluate the density (ρ_{nf}), heat capacity ($C_{p_{nf}}$),

$$\rho_{nf} = (1 - \phi)\rho_f + \phi\rho_p \quad (11)$$

$$C_{p_{nf}} = \frac{(1 - \phi)C_{p_f}\rho_f + \phi C_{p_p}\rho_p}{\rho_{nf}} \quad (12)$$

$$\beta_{nf} = \frac{(1 - \phi)\beta_f\rho_f + \phi\beta_p\rho_p}{\rho_{nf}} \quad (13)$$

$$M_{nf} = (1 - \phi)M_f + \phi M_p \quad (14)$$

The second viscosity model presented in Table 2 was acquired experimentally for the nanofluid that was obtained at nanoparticle volumetric fractions varying in the range from 0.33% to 5% with 43 nm Al_2O_3 nanoparticles and the water based fluid. A Brookfield cone and plate viscometer was utilized. Whereas an increase occurred in the nanofluid viscosity along with the nanoparticle volumetric fraction in case of the highest nanoparticle volumetric fraction of 2%, a nonlinear correlation was demonstrated between the increased nanofluid viscosity and nanoparticle volumetric fraction in case of the nanoparticle volumetric fraction higher than 2%. The cause of the mentioned situation above may be due to more considerable hydrodynamic interaction between particles in case of the nanoparticle volumetric fraction above 2%. The third viscosity model in Table 2 represents the correlation equation acquired for the nanofluid at various nanoparticle volumetric fractions (1-5%), established experimentally in the current research with 80 nm Al_2O_3 nanoparticles and the water based fluid. Moreover, the model employed as the thermal conductivity model represents the effective thermal conductivity model suggested by Maxwell in theoretical terms.

3. RESULTS AND DISCUSSION

In this study, contour plots of stream function and dimensionless temperature isotherms of Al_2O_3 -water nanofluid at various nanoparticle volumetric fractions and different Re and Gr numbers were studied in a square cavity geometry. Stream function and temperature contour values were obtained for nanoparticle volumetric fractions of 0%, 3%, and 5% with Model 1, Model 2, and Model 3. In Figure 2, the cases when the Re number was 100 and the Gr number

thermal expansion coefficient (β_{nf}), and molecular weight (M_{nf}) of the Al_2O_3 -water nanofluid:¹³

was 10^3 , 10^4 , and 10^5 at different nanoparticle volumetric fractions were examined for Model 1. In case when the Gr number is 10^3 , a flow occurs in the square cavity geometry due to the movement of the upper plate, and the primary vortex (eddy) is formed in the center of the geometry. In case when the Gr number is 10^4 , the secondary vortex occurs in the lower right corner at the constant nanoparticle volumetric fraction. The reason for the formation of the secondary vortex is stagnation pressure and friction losses. The primary vortex occurs in the center of the square cavity geometry, while the secondary vortices occur in the corners resulting from the movement of upper plate and in the direction in which the plate moves. Another smaller vortex occurs when the Gr number is 10^5 in the lower left corner of the geometry. The reason for the formation of the tertiary vortex is the formation of a negative pressure gradient. At the constant nanoparticle volumetric fraction and constant Re number, the number Ri increases with the increased Gr number. With the increase in the Re number at the constant Gr number, the Ri number will decrease, and forced convection heat transfer will become more dominant. Contrary to this situation, with the increase in the Gr number at the constant Re number, the Ri number will also increase, and natural convection heat transfer will become more dominant. In Figure 2, when the Gr number was 10^5 , the primary vortex formed in the center shrank, and the secondary vortex formed in the lower right corner grew. In this case, natural convection heat transfer became more dominant. In the case when the nanoparticle volumetric fraction was 3% and the Gr number was 10^3 , only a large vortex was observed in the center, and when the Gr number increased to 10^5 , a large vortex occurred in the lower right corner, and a tertiary vortex was formed in the lower left corner.

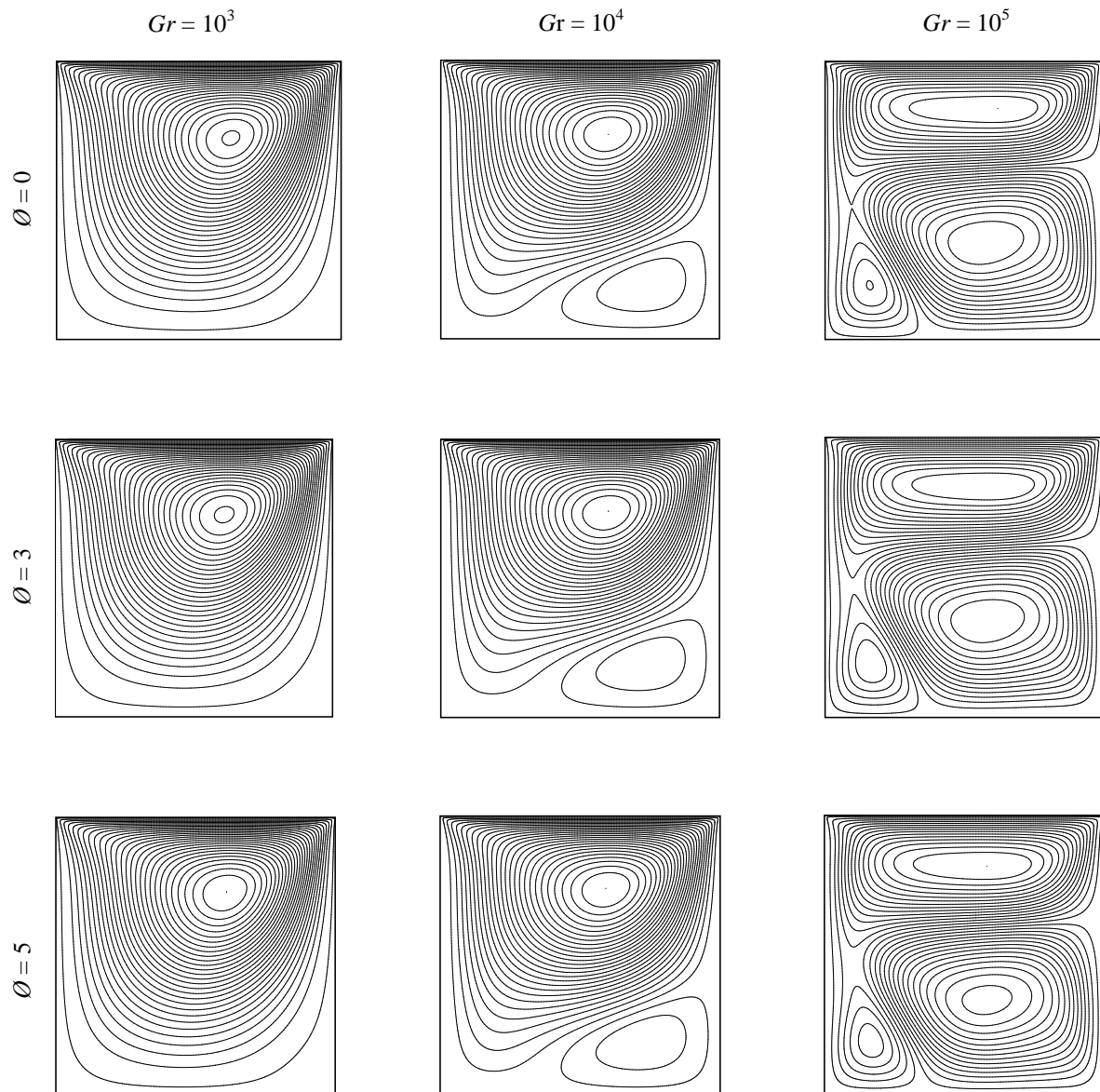


Figure 2. Plots of stream function contours obtained at the Re number of 100 and the Gr numbers of 10^3 , 10^4 , and 10^5 from Model 1 at different nanoparticle volumetric fractions.

It is thought that the secondary vortex occurs because of heat transfer, and the effect of natural convection increases with the formation of the secondary vortex. No change is observed in the primary and secondary vortices with the increased nanoparticle volumetric fraction at the constant Gr number. According to the conclusions drawn in Figure 2, it is understood that the heat transfer at low Ri numbers occurs with forced convection and the increase in the nanoparticle volumetric fraction does not have an impact on the stream function contours, and the increase in the nanoparticle volumetric fraction does not have a significant impact on the flow when natural convection

heat transfer occurred. In Figure 3, dimensionless temperature isotherms are observed at different Gr numbers and different nanoparticle volumetric fractions at the constant Re number for Model 1. In Figure 3, as the Gr number increases at the constant nanoparticle volumetric fraction in dimensionless temperature isotherms of the Al_2O_3 -water nanofluid in the square cavity geometry, the thermal boundary layer thickens and becomes frequent since the secondary vortex will also increase, and heat transfer occurs by natural convection, as can be clearly observed when the Gr number becomes 10^5 . In case when the Gr number is 10^3 , the thermal boundary layer gets very close to the

walls of the square cavity geometry, and this is an indication of forced convection heat transfer, and the

medium in the main region of the geometry is almost isothermal.

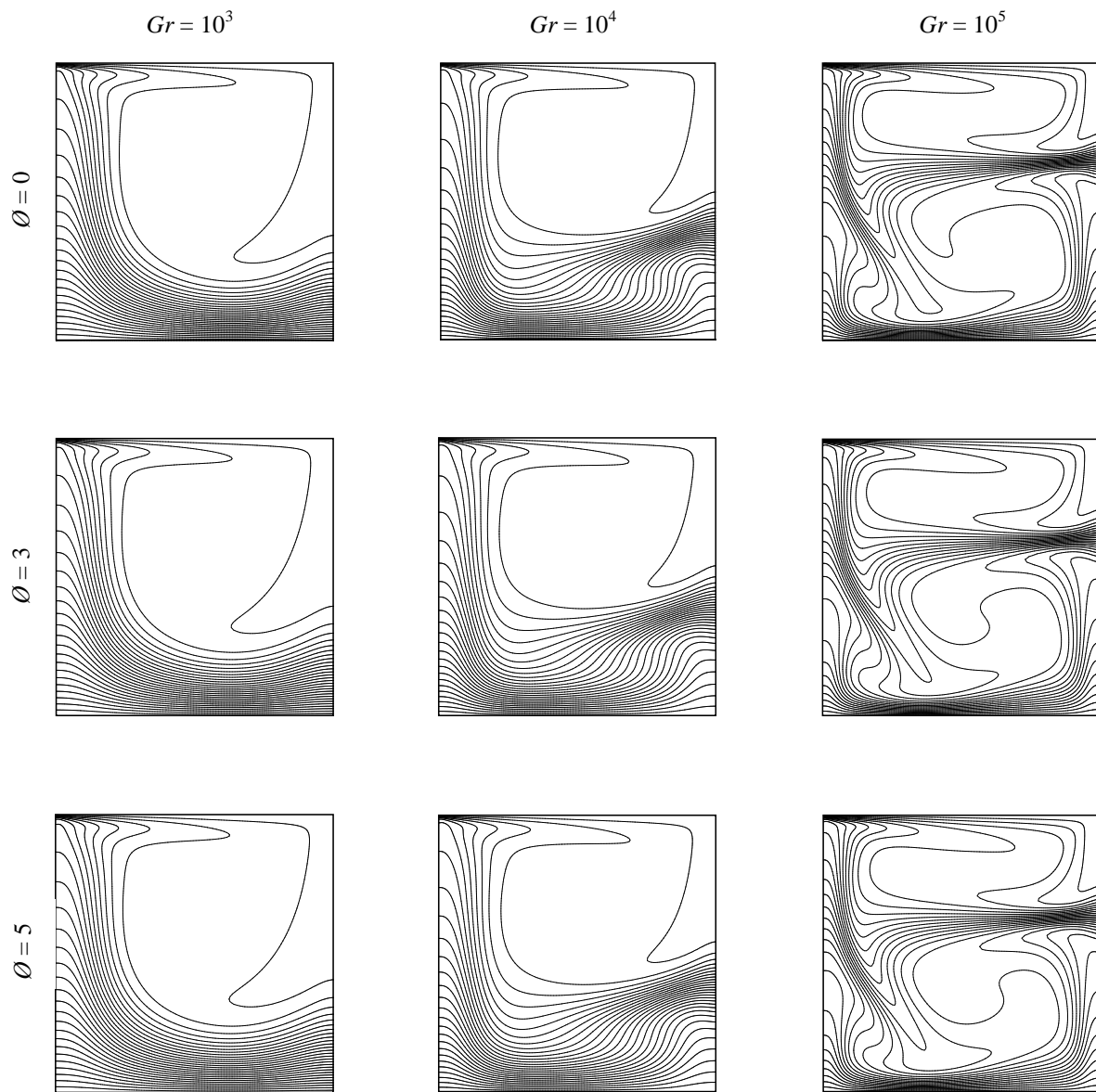


Figure 3. Plots of isotherms obtained at the *Re* number of 100 and *Gr* numbers of 10^3 , 10^4 , and 10^5 from Model 1 at different nanoparticle volumetric fractions.

In Figure 4, the cases when the *Re* number was 100 and the *Gr* number was 10^3 , 10^4 , and 10^5 at different nanoparticle volumetric fractions for Model 2 were examined. When the *Gr* number was 10^3 , the primary vortex (eddy) occurred in the center of the geometry. In this case, the primary vortex was not affected much by the increase in the nanoparticle volumetric fraction, and a very small amount of decrease in the size of the vortex was observed. Since there is movement here, in other words, there is forced convection heat transfer, the primary vortex did not show much change with the

increased nanoparticle volumetric fraction because the movement of the nanofluid is more dominant. The secondary vortex that is heat-induced is not affected because the primary vortex, which is movement-induced, is much more dominant. When the *Re* number was 100 and the *Gr* number was 10^4 , the size and width of the secondary vortex were observed to decrease slightly with the increased nanoparticle volumetric fraction. The secondary vortex decreases with the nanoparticle volumetric fraction that increases with the increasing *Gr* number. Because the viscosity of the

nanofluid will increase here, the movement is restricted, and the heat transfer due to natural convection decreases. A similar situation arises when the Re number is 100 and the Gr number is 10^5 . Here, the size and width of the tertiary vortex also decrease with the increasing nanoparticle volumetric fraction.

Unlike Model 2, any change was not observed in stream function values with the increasing nanoparticle

volumetric fraction in Model 1. Model 1 is the model created by the combination of the models of Einstein as a viscosity model and Maxwell as a thermal conductivity model and is a traditionally common model in the literature. In case when Model 1 was used in natural convection heat transfer, no alteration in the heat transfer rate was observed with the increased nanoparticle volumetric fraction.

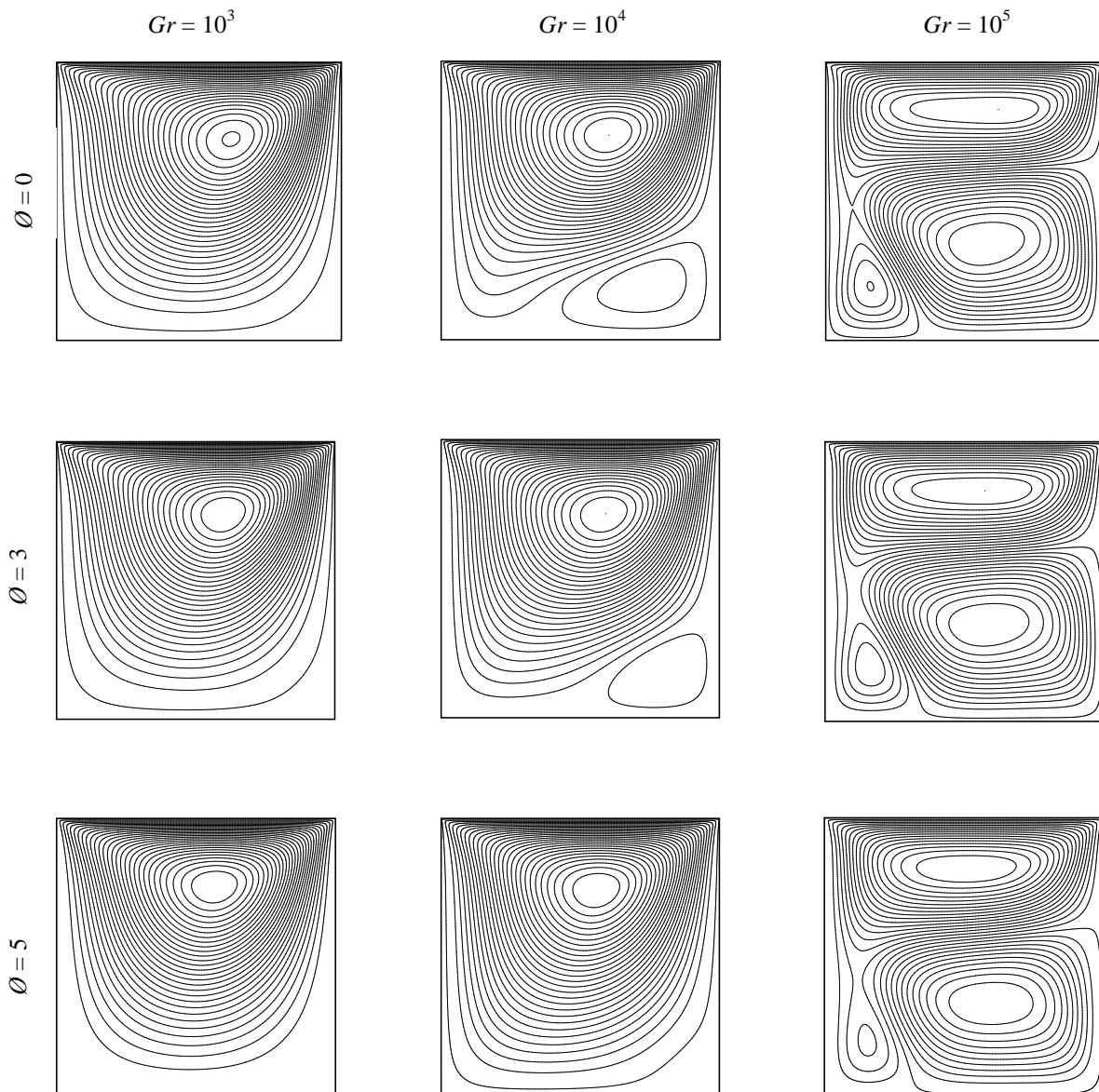


Figure 4. Plots of stream function contours obtained at the Re number of 100 and the Gr numbers of 10^3 , 10^4 , and 10^5 from Model 2 at different nanoparticle volumetric fractions.

In **Figure 5**, dimensionless temperature isotherms are observed at different Gr numbers and different nanoparticle volumetric fractions at the constant Re number for Model 2. In **Figure 5**, as the Gr number increases at the constant nanoparticle volumetric

fraction in the dimensionless temperature isotherms of the Al_2O_3 -water nanofluid in the square cavity geometry, the thermal boundary layer thickens and becomes frequent since the secondary vortex will also increase, and heat transfer occurs by natural convection,

as can be clearly observed when the Gr number is 10^5 . In case when the Gr number is 10^3 , the thermal boundary layer gets very close to the walls of the square cavity geometry, and this is an indication of forced convection heat transfer, and the medium in the main

region of the geometry is almost isothermal. In case when the Gr number is 10^4 , it was revealed that the isothermal image formed in the center disappeared with the increased nanoparticle volumetric fraction, and the impact of natural convection heat transfer was observed.

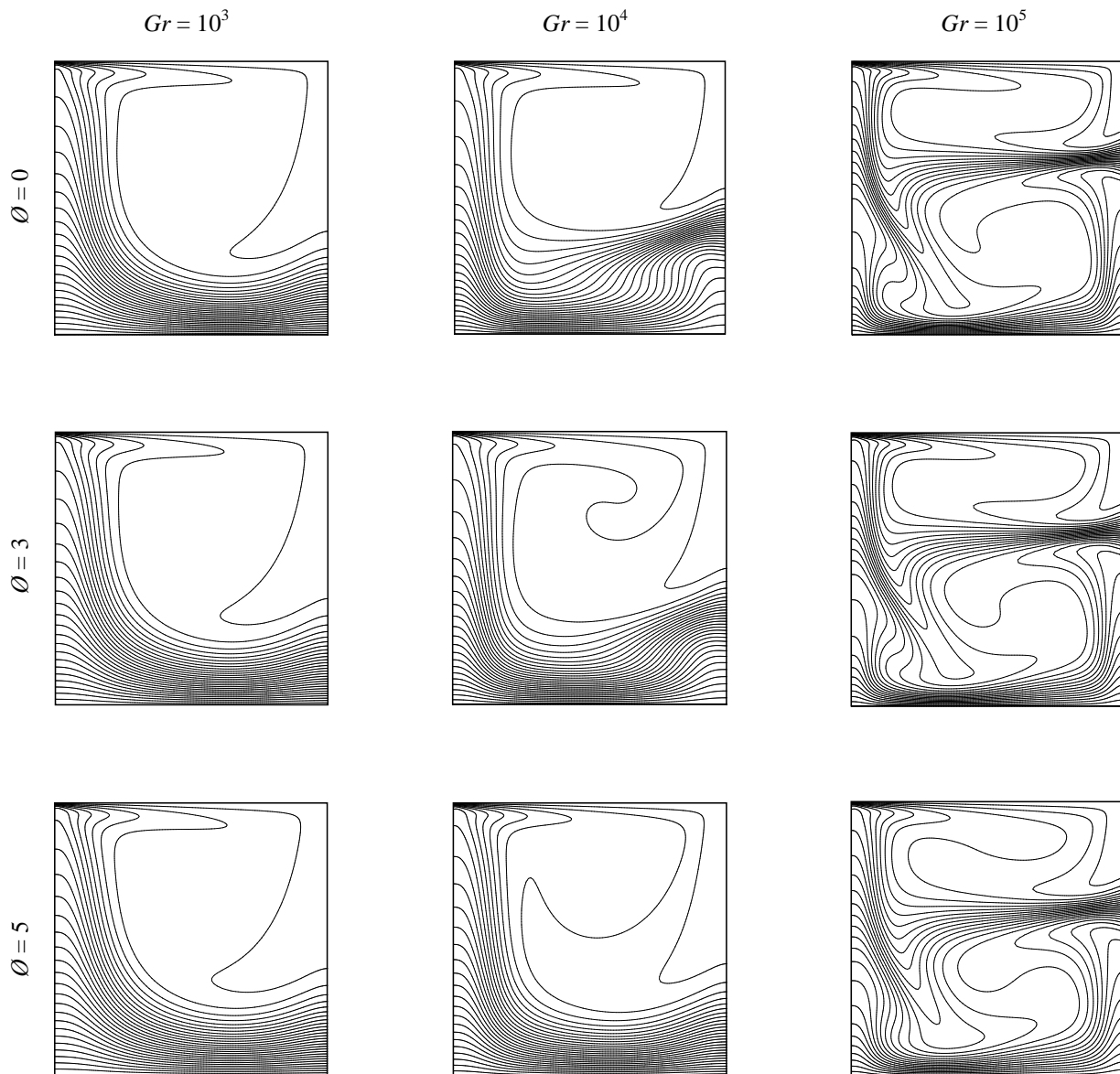


Figure 5. Plots of isotherms obtained at the Re number of 100 and the Gr numbers of 10^3 , 10^4 , and 10^5 from Model 2 at different nanoparticle volumetric fractions.

In Figure 6, the cases when the Re number was constant and 100 and the Gr number was 10^3 , 10^4 , and 10^5 at different nanoparticle volumetric fractions for Model 3 were examined. In case when the Gr number is 10^3 , a flow occurs in the square cavity geometry due to the movement of the upper plate, and a primary vortex occurs in the center of the geometry. While heat transfer is realized by the forced convection mechanism at a low Gr number at the constant Re number and constant

nanoparticle volumetric fraction, it is clearly observed to be realized by natural convection mechanism at high Gr numbers at the constant Re number and constant nanoparticle volumetric fraction. The primary vortex was almost unaffected by the increase in the nanoparticle volumetric fraction in case when the Re number was constant and the Gr number was 10^3 . This is an expected situation because, although the viscosity of the nanofluid would increase with the increase in the

presence of nanoparticles in the medium, the movement of the nanoparticle was not influenced since the forced convection heat transfer here was more dominant than natural convection heat transfer, and no change was observed in the size and width of the stream function values. In the second case, it was observed that the size and width of the secondary vortex formed in the lower right corner decreased slightly with the increased nanoparticle volumetric fraction in case when the Re number was constant and the Gr number was 10^4 . The

secondary vortex decreases with the nanoparticle volumetric fraction increasing with an increase in the Gr number because, since the viscosity of the nanofluid will increase here, the movement will be restricted, and natural convection heat transfer will be decreased. A similar situation arises when the Re number is 100 and the Gr number is 10^5 . Here, the size and width of the tertiary vortex also decrease with increasing nanoparticle volumetric fraction.

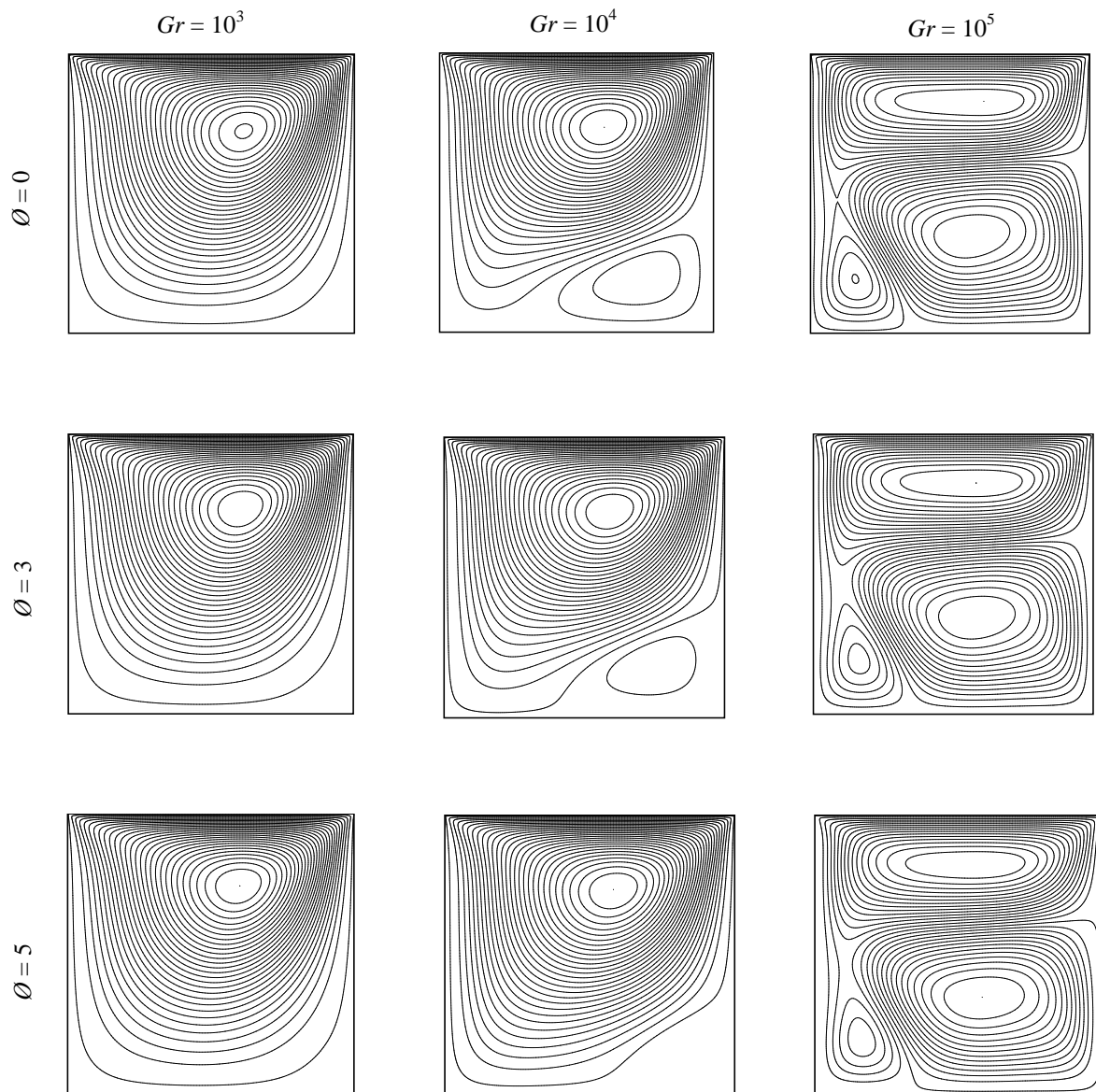


Figure 6. Plots of stream function contours obtained at the Re number of 100 and the Gr numbers of 10^3 , 10^4 , and 10^5 from Model 3 at different nanoparticle volumetric fractions.

In Figure 7, dimensionless temperature isotherms are observed at different Gr numbers and different nanoparticle volumetric fractions at the constant Re number for Model 3. In Figure 7, as the Gr number increases at the constant nanoparticle volumetric fraction in the dimensionless temperature isotherms of the Al_2O_3 -water nanofluid in the square cavity geometry, the thermal boundary layer thickens and becomes frequent since the secondary vortex will also increase, and heat transfer occurs by natural convection, as can be clearly observed when the Gr number is 10^5 .

In case when the Gr number is 10^3 , the thermal boundary layer gets very close to the walls of the square cavity geometry, and this is an indication of forced convection heat transfer, and the medium in the main region of the geometry is almost isothermal. In case when the Gr number is 10^4 , unlike the case that occurs in Model 2, it is clearly observed that the isothermal image in the main region of the geometry has not disappeared yet even at the moment when the nanoparticle volumetric fraction is 3%.

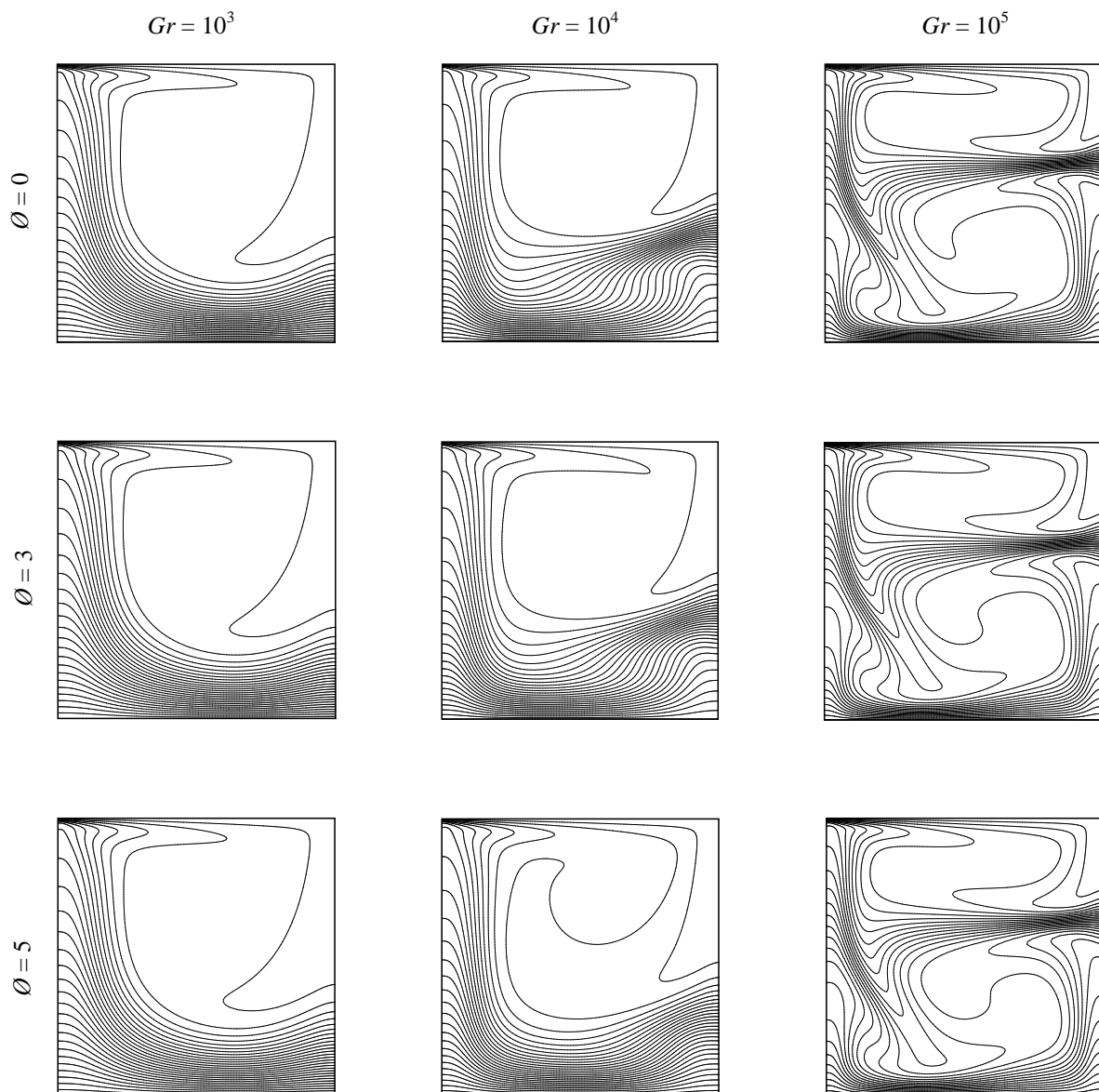


Figure 7. Plots of isotherms obtained at the Re number of 100 and the Gr numbers of 10^3 , 10^4 , and 10^5 from Model 3 at different nanoparticle volumetric fractions.

In Figure 8, both natural and forced convection heat transfer stream function in the square cavity geometry are demonstrated in cases when the Re numbers are 10,

100, and 1000 and the Gr numbers are 10^3 , 10^4 , and 10^5 and the Al_2O_3 -water nanofluid concentrations are 0%, 3%, and 5% for Model 3. In case when the Re number is

10, the number of vortexes formed in the square cavity geometry increased with the increased Gr number. Here, it is observed that only one vortex is formed in the center when the Re number is 10 and the Gr number is 10^3 , that a small increase occurs in the size and width of the vortex when the Gr number is 10^4 , and that in the final case, a large secondary vortex occurs in the lower right corner under the effect of natural convection when the Gr number is 10^5 . Furthermore, in the final case,

when the Re number was 10 and the Gr number was 10^5 , the effect of the nanoparticle volumetric fraction emerged. It is noteworthy that in the case when the Re number is 1000, the size and width of the stream function contours are almost the same at all Gr numbers. Here, since forced convection heat transfer is more dominant, no secondary vortex occurs anywise, while a shift in the vortex towards the upper right corner is observed due to the movement of the upper plate.

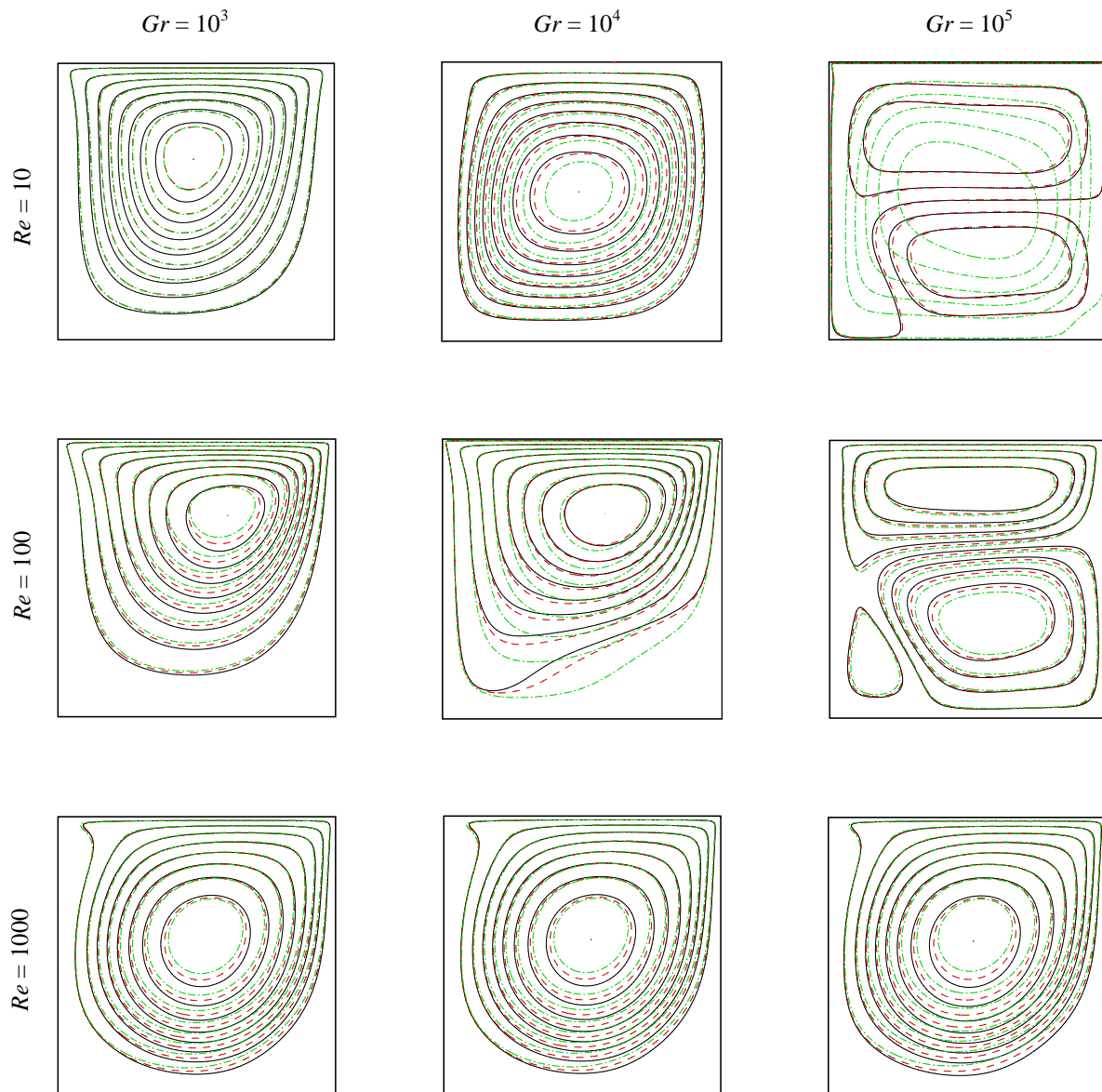


Figure 8. Plots of stream function contours obtained at the Re numbers of 10, 100, and 1000 and the Gr numbers of 10^3 , 10^4 , and 10^5 from Model 3 at different nanoparticle volumetric fractions. Straight line: Base fluid pure water; Dashed line: volumetric fraction $\phi = 3\%$, Dot-dashed line: volumetric fraction $\phi = 5\%$.

In **Figure 9**, both natural and forced convection heat transfer dimensionless temperature isotherms in the square cavity geometry are demonstrated in cases when the Re number is 10, 100, and 1000 and the Gr number

is 10^3 , 10^4 , and 10^5 and the Al_2O_3 -water nanofluid concentration is 0%, 3%, and 5% for Model 3. In the square cavity geometry, since the secondary vortex will increase as the Gr number increases in case when the Re

number is constant and 10 in the dimensionless temperature isotherms of the Al₂O₃-water nanofluid, the thermal boundary layer thickens and becomes frequent, and heat transfer is realized by natural convection as it is clearly observed when the *Gr* number is 10⁵. At low *Gr* numbers, heat transfer takes place here by natural convection, and the isotherms progress almost parallel to the horizontal walls. In case when the *Re* number is 100 and the *Gr* number is 10⁴, both natural and forced convection heat transfer occurs, and while the medium

in the center of the geometry is isothermal, thermal boundary layers are observed to be formed on the walls. At the *Re* number of 1000 and at all values of the *Gr* number, forced convection heat transfer occurs, as can be clearly observed from the dimensionless temperature isotherms, and the thermal boundary layer gets very close to the walls of the square cavity geometry, and the medium in the main region of the geometry becomes almost isothermal.

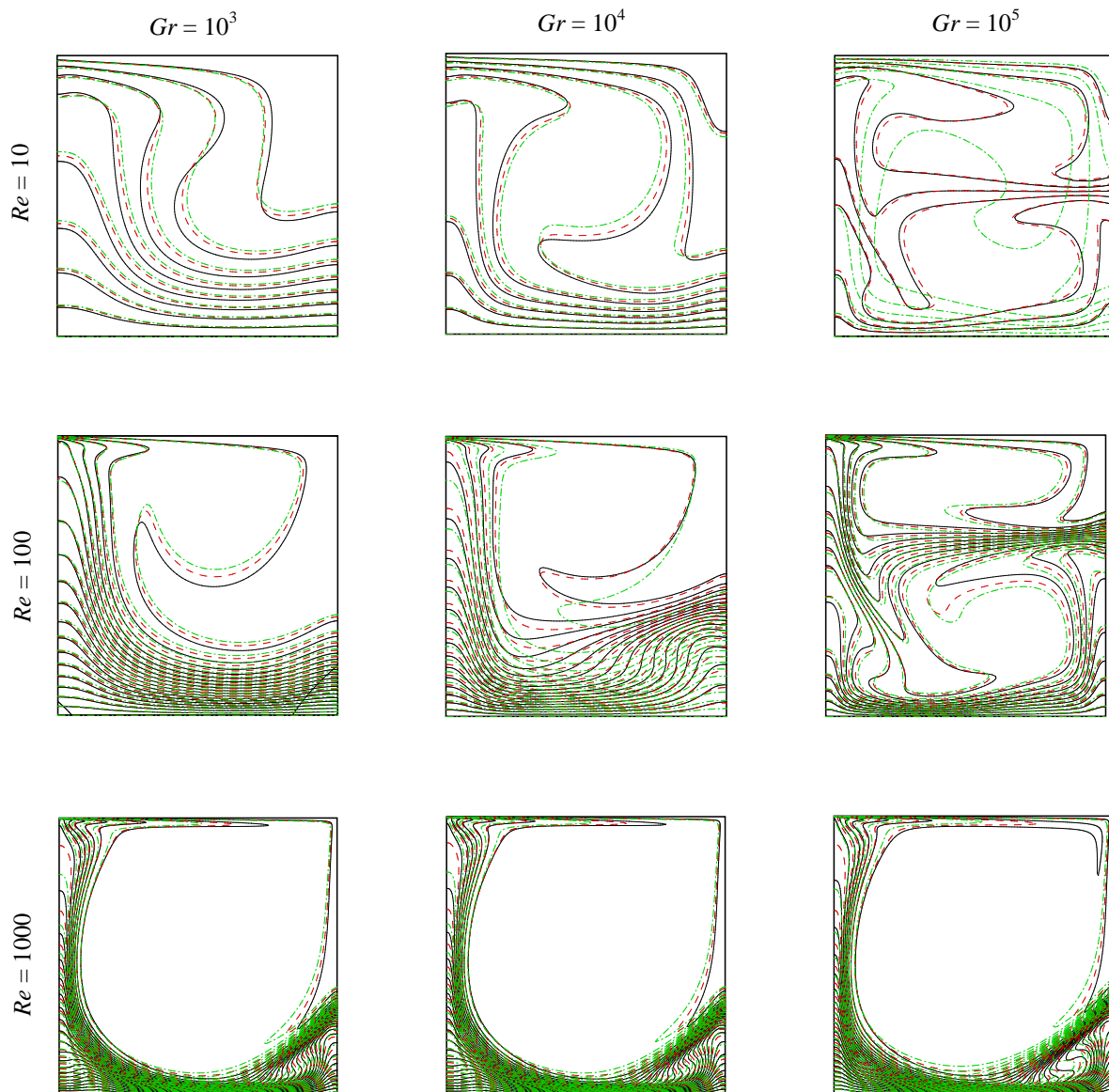


Figure 9. Plots of isotherms obtained at the *Re* numbers of 10, 100, and 1000 and the *Gr* numbers of 10³, 10⁴, and 10⁵ from Model 3 at different nanoparticle volumetric fractions. Straight line: Base fluid pure water; Dashed line: volumetric fraction $\phi = 3\%$, Dot-dashed line: volumetric fraction $\phi = 5\%$.

The results obtained from the numerical solution are presented in Tables 3, 4 and 5 as the average *Nu* results obtained along the hot wall in Models 1, 2, and 3 for the

Gr numbers in the range of 10³ - 10⁵, the *Re* numbers of 10 - 100 - 1000, and the nanoparticle volumetric fraction of 0-5%. The increase in heat transfer rate at

DOI: <http://dx.doi.org/10.32571/ijct.697728>

E-ISSN:2602-277X

high nanoparticle volumetric fractions and at constant Gr numbers indicates significant changes depending on the Re number. Furthermore, it is observed from the tables that the average Nu number increases

significantly with the decreasing Ri number at constant nanoparticle volumetric fractions in all models. The results obtained are compatible with similar studies in the literature.¹⁵⁻¹⁹

Table 3. The average Nu results obtained along the hot wall for the Al_2O_3 -water nanofluid as a result of both natural and forced convection for Model 1 in the square cavity geometry

MODEL 1									
θ	$Gr 10^3$			$Gr 10^4$			$Gr 10^5$		
	Re			Re			Re		
	10	100	1000	10	100	1000	10	100	1000
0	2.69424404	4.48216182	13.94232762	4.24429466	4.14744341	14.01411223	4.75732946	6.53374570	14.51737682
1	2.73408941	4.54370984	14.03291625	4.32616103	4.21598073	14.10101304	4.96577250	6.66038678	14.53190419
3	2.80761521	4.66156512	14.11548359	4.48450498	4.35206376	14.18134660	5.19772318	6.90535801	14.36249305
5	2.87274283	4.77296707	14.05252179	4.63587590	4.48875865	9.55710989	5.42329901	7.13869699	13.72670099

Table 4. The average Nu results obtained along the hot wall for the Al_2O_3 -water nanofluid as a result of both natural and forced convection for Model 2 in the square cavity geometry

MODEL 2									
θ	$Gr 10^3$			$Gr 10^4$			$Gr 10^5$		
	Re			Re			Re		
	10	100	1000	10	100	1000	10	100	1000
0	2.69424404	4.48216182	13.94232762	4.24429466	4.14744341	14.01411223	4.75732946	6.53374570	14.51737682
1	2.74035660	4.54778487	14.06456215	4.33511274	4.20498721	14.13614101	4.87869860	6.67723320	14.56513756
3	2.68805410	4.59871794	13.46401055	4.32049297	4.76506117	13.53830100	4.89155483	6.59627443	13.77169901
5	2.43470817	4.59902274	11.70808334	4.02832936	5.34386604	11.79175418	6.24078071	6.01816599	12.00956067

Table 5. The average Nu results obtained along the hot wall for the Al_2O_3 -water nanofluid as a result of both natural and forced convection for Model 3 in the square cavity geometry

MODEL 3									
θ	$Gr 10^3$			$Gr 10^4$			$Gr 10^5$		
	Re			Re			Re		
	10	100	1000	10	100	1000	10	100	1000
0	2.69424404	4.48216182	13.94232762	4.24429466	4.14744341	14.01411223	4.75732946	6.53374570	14.51737682
1	2.72827432	4.54002029	13.99495980	4.31779231	4.22755615	14.06804469	4.85857939	6.64466637	14.50105043
3	2.75616969	4.63292033	13.83614958	4.41330144	4.47238444	13.90617540	5.00065179	6.77172960	14.10992917
5	2.84253633	4.70846295	13.36343161	4.45543648	5.10934326	13.42201614	6.98341032	6.80042011	13.22567790

4. CONCLUSIONS

In this study, both natural and forced convection heat transfer of the Al_2O_3 - water nanofluid were examined in the square cavity geometry where the upper wall moved at a certain constant velocity, the other walls were immobile, the lower wall was heated, the upper wall was cooled, and the side walls were insulated. As a result of the numerical solution, the maximum, minimum Re and Gr numbers and average Nu number, and stream function and dimensionless temperature isotherms were examined in Models 1, 2, and 3 for the Gr number in the range of $10^3 - 10^5$, the Re number of 10 - 100 - 1000, and the nanoparticle volumetric fraction 0%, 3%, and 5%, and the following conclusions were reached:

- An investigation of the mixed convection heat transfer of an Al_2O_3 -water nanofluid was carried out at the constant Grashof number and altering Reynolds number, and with the order reversed. It was determined that enhancement occurred in heat transfer at the constant Grashof number of 10^4 with nanoparticle concentration for the Reynolds numbers as low as 100. Nevertheless, enhancement occurred in heat transfer at the Reynolds number of 1000 with nanoparticle volume fractions reaching 0.01. Increasing the nanoparticle concentration even further causes a decrease in heat transfer.
- An increase in heat transfer took place with nanoparticle concentration at the constant Reynolds number of 100 and the low Grashof number of 10^3 . Nevertheless, at the constant Reynolds number of 1000 and the high Grashof number of 10^5 , the highest heat transfer was determined at the concentration of 0.01, and following the mentioned concentration, the performance of heat transfer got worse in comparison with the base fluid not containing nanoparticles.
- The average Nu number, which represents a measure of heat transfer in Models 1, 2, and 3 at constant Re numbers and calculated from the heated wall, was determined to increase with the increasing Re number.
- A decrease in heat transfer was revealed with the increasing Gr number at low Gr number values and at constant Re numbers. It was revealed that the reason for this was the realization of heat transfer by the natural convection mechanism as a result of the increase in the Ri number as the Gr number increases at constant Re numbers.
- In Models 1, 2, and 3, the average Nu number was found to increase significantly with the decrease in the Ri number at constant nanoparticle volumetric fractions.
- As a result, both natural and forced convection heat transfer of nanofluids in the square cavity geometry were demonstrated to change depending on the

nanoparticle volumetric fraction, Re and Gr numbers.

ACKNOWLEDGEMENTS

The Scientific Research Project Fund of Sivas Cumhuriyet University provided its support for the present research under the project number M-489.

Conflict of interests

Authors declare that there is no a conflict of interest with any person, institute, company, etc.

REFERENCES

1. Esfe, M. H.; Saedodin, S.; Malekshah, E. H.; Babaie, A.; Rostamian, H. *J. Therm. Anal. and Calorim.* **2019**, *135* (1), 813-859.
2. Tiwari, R. K.; Das, M. K. *Int. J. Heat Mass Transf.* **2007**, *50*, 2002-2018.
3. Talebi, F.; Mahmoudi, A. H.; Shahi, M. *Int. Commun. Heat Mass Tran.* **2010**, *37* (1), 79-90.
4. Arefmanesh, A.; Mahmoudi, M. *Int. J. Therm. Sci.* **2011**, *50* (9), 1706-1719.
5. Brinkman, H. C. *J. Chem. Phys.* **1952**, *20* (4), 571-582.
6. Maiga, S. E. B.; Nguyen, C. T.; Galanis, N.; Roy, G. *Heat transfer enhancement in forced convection laminar tube flow by using nanofluids*, Proceedings of the International Symposium on Advances in Computational Heat Transfer III, Paper CHT-040101, p. 24, Begell House Publishers, 2004.
7. Chamkha, A. J.; Rashad, A. M.; Armaghani, T.; Mansour, M. A. *J. Therm. Anal. Calorim.* **2018**, *132* (2), 1291-1306.
8. Kapil, M.; Roy, D., Sharma, B., Rana, S. C., Pramanik, S., Barman, R. N. *Mater. Today-Proc.* **2019**, *11*, 700-707.
9. Abu-Nada, E.; Masoud, Z.; Hijazi, A. *Int. Commun. Heat Mass Tran.* **2008**, *35* (5), 657-665.
10. Kim, C. S.; Okuyama, K.; Fernández de la Mora, J. *Aerosol Sci. Tech.* **2003**, *37* (10), 791-803.
11. Yapici, K.; Obut, S. *Int. J. Numer. Method H.* **2015**, *25* (5), 998-1029.
12. Einstein, A. *Investigations on the theory of the Brownian movement*, Dover Books, 1956.


DOI: <http://dx.doi.org/10.32571/ijct.697728>


E-ISSN:2602-277X

13. Maxwell, J.C. *A Treatise on Electricity and Magnetism*. Third ed Clarendon Press, Oxford, 1904.
14. Chandrasekar, M.; Suresh, S.; Chandra Bose, A. *Exp. Therm. Fluid Sci.* **2010**, 34 (2), 210-216.
15. Ögüt, E. B.; Kahveci, K. *J. Mol. Liq.* **2016**, 224, 338-345.
16. Yapıcı, K.; Obut, S. *Heat Transfer Eng.* **2015**, 36 (3), 303-314.
17. Heydari, M. R.; Esfe, M. H.; Hajmohammad, M. H.; Akbari, M.; Esforjani, S. S. M. *Heat Transf. Res.* **2014**, 45 (1), 75-95.
18. Taamneh, Y.; Bataineh, K., *Stroj. Vestn-J. Mech. E.* **2017**, 63 (6), 383-393.
19. Lauriat, G. *Appl. Therm. Eng.* **2018**, 129, 1039-1057.

ORCID

 <https://orcid.org/0000-0002-8634-9232> (N. Keklikcioğlu Çakmak)

 <https://orcid.org/0000-0003-2454-7003> (H. H. Durmazuçar)

 <https://orcid.org/0000-0002-3902-9375> (K. Yapıcı)